Article:
Wang, C. orcid.org/0000-0003-0791-4238, Sheng, B., Li, Z. orcid.org/0000-0003-2583-5082 et al. (4 more authors) (2023) A Lightweight Series Elastic Actuator With Variable Stiffness: Design, Modeling, and Evaluation. IEEE/ASME Transactions on Mechatronics, 28 (6). pp. 3110-3119. ISSN 1083-4435

https://doi.org/10.1109/tmech.2023.3254813

A Lightweight Series Elastic Actuator With Variable Stiffness: Design, Modeling, and Evaluation

Chao Wang, Bo Sheng, Zhenhong Li, *Member, IEEE*, Manoj Sivan, Zhi-Qiang Zhang, *Member, IEEE*, Gu-Qiang Li, and Sheng Quan Xie, *Senior Member, IEEE*

***Abstract*—This article proposes a lightweight variable stiffness actuator (LVSA) driven by a novel mechanism with four sliders on a shared crank (FS2C). The FS2C mechanism allows the LVSA to simultaneously regulate the preload of four springs using only one motor and hence achieves a wider-range continuous stiffness adaption with reduced weight. A cable transmission system is developed to remotely place motors and further reduce the influence of the LVSA on the mass distribution. A dynamics model is established to study the torque-deflection and the stiffness-deflection relations. Based on the model, a torque-stiffness controller is proposed. Experiments are carried out to validate the performance of the dynamics model, the controller, and the LVSA. The results indicate that the LVSA provides a range of stiffness from 0 to 988 Nm/rad with a weight of 0.412 kg, and the controller is accurate in adjusting the output torque and stiffness at relatively high speeds. The proposed actuator provides a solution for actuation systems that have to be lightweight with variable stiffness, such as wearable robotics and assistive exoskeletons.**

***Index Terms*—Bowden cable transmission, exoskeleton, rehabilitation, series elastic actuator.**

Manuscript received 26 October 2022; revised 23 January 2023; accepted 6 March 2023. Recommended by Technical Editor Z. Bi and Senior Editor W.J. C. Zhang.This work was supported in part by U.K. EPSRC under Grants EP/V057782/1 and EP/S019219/1. This work was conducted in the Institute of Rehabilitation Engineering, Binzhou Medical University, Yantai, 264033, China. *(Corresponding authors: Gu Qiang Li; Sheng Quan Xie; Zhenhong Li.)*

Chao Wang, Zhenhong Li, and Zhi-Qiang Zhang are with the School of Electrical and Electronic Engineering, University of Leeds, LS2 9JT Leeds, U.K. (e-mail: elcw@leeds.ac.uk; Z.H.Li@leeds.ac.uk; Z.Zhang3@leeds.ac.uk).

Bo Sheng is with the School of Mechatronic Engineering and Automation, Shanghai University, Shanghai 20044, China (e-mail: shengbo@shu.edu.cn).

Manoj Sivan is with the Academic Department of Rehabilitation Medicine, University of Leeds, LS2 9JT Leeds, U.K. (e-mail: m.sivan@leeds.ac.uk).

Gu-Qiang Li is with the Institute of Rehabilitation Engineering, Binzhou Medical University, Yantai 264033, China (e-mail: lgq100@bzmc.edu.cn).

Sheng Quan Xie is with the School of Electronic and Electrical Engineering, University of Leeds, LS2 9JT Leeds, U.K., and also with the Institute of Rehabilitation Engineering, Binzhou Medical University, Yantai 264033, China (e-mail: s.q.xie@leeds.ac.uk).

Color versions of one or more figures in this article are available at https://doi.org/10.1109/TMECH.2023.3254813.

Digital Object Identifier 10.1109/TMECH.2023.3254813

I. Introduction

EXOSKELETON robots have been developed to assist rehabilitation training in recent years [1], [2], [3], [4]. To achieve effective physical human–robot interaction (pHRI), robot actuators should have compliance to address safety concerns [5], [6], [7]. Two strategies are widely used to provide compliance: 1) active strategy [8], [9], [10] and 2) passive strategy [11], [12], [13]. The active strategy uses force/torque feedback and control algorithms to emulate compliant behavior without adding compliant components. However, the active strategy cannot guarantee safe interaction when sensor fails [14].

Different from the active strategy, the passive strategy provides inherent compliance with low mechanical impedance by introducing elastic components [11], [12], [13]. In addition, the inherent compliance allows the force/torque control to be converted to a position control, which can improve the force/torque tracking performance. The existing passive compliant actuators can be categorized into fixed stiffness actuators (FSAs) and variable stiffness actuators (VSAs).

FSAs typically use a fixed mechanical configuration of rigid segments and elastic elements with one single dc motor to control the output, e.g., [15], [16], [17]. The compliant behaviors of FSAs are normally designed based on a preset working condition, which limits the response bandwidth, torque control accuracy, energy storage capacity, and dynamical adaptability with environments. Hence, VSAs are developed to address these issues with an additional motor for stiffness regulation. There are various stiffness regulation strategies used by VSAs: 1) changing preload of spring, e.g., MACCEPA 2.0 [13], SVSA [18], JASR [14], and RVSA [19]; 2) changing the transmission ratio between springs and the actuator output, e.g., AwAS-II [12], [20], REGT-VSA [21], vsaUT-II [44], and [22], [23], [24]; and 3) changing the physical properties of the elastic element, e.g., "Jack-Spring" [25], S-Shaped Spring [26], and [27] Pneumatic VSAs were proposed in the previous studies [28], [29]. The stiffness is regulated by changing the pressure of gas which is similar to changing the preload of spring. Variable stiffness improves the adaptability of actuators to different scenarios; however, additional mechanisms and a secondary motor are required to adjust the stiffness, which increases the design complexity and weight of VSAs compared with FSAs. Changing

the transmission ratio aims to adjust the moment arm vector in the definition of torque, and VSAs based on this strategy normally use ball screw or a group of gears to change the pivot point, which makes the mechanism bulky and heavy. Changing the physical properties of the elastic element can be achieved in material and mechanism, while existing VSAs based on strategy 1) and 2) demonstrated more advantages than those with strategy 3) with regard to weight and size [30]. Among the three strategies, VSAs based on changing preload are normally lighter and have better compatibility and smoother stiffness regulation than others. Nevertheless, the VSAs based on changing preload generally use a single elastic element, which may limit its range of stiffness. Multiple elastic elements are adopted by VSAs based on other principles, which however, increases the complexity of the stiffness adjustment mechanism [26], [31].

To minimize the influence of joint actuator on body mass distribution, the weight of the actuator should be as light as possible. Previous studies used dc motors with gears or hydraulic mechanisms to directly drive human joints [32], [33], [34], [35]. However, installing dc motors or high mass mechanisms on human joints will affect the body mass distribution and increase the moment inertia, especially for the distal joints. Previous studies showed that by employing the Bowden cable transmission with motors remotely placed, exoskeletons can achieve low worn mass and high output torque [36], [37], [38], [39], [40], [41].

In this study, we propose a cable-driven lightweight VSA (LVSA) based on the principle of changing the spring preload. The LVSA employs four parallel springs with a novel mechanism with four sliders on a shared crank (FS2C) which achieves wide-range stiffness adaption with one additional motor. The contributions of this article are summarized as follows.

1) A novel mechanism named FS2C is proposed to adjust the preload of springs, by which a light-weight VSA is designed. Compared with the previous designs using multiple elastic elements [26], [31], the proposed LVSA adjusts the stiffness with a simpler mechanism, which reduces the weight of the actuator.
2) A dynamics model is established to describe the torque-deflection and stiffness-deflection relations of the LVSA, which is implemented in the torque-stiffness control. The torque-stiffness estimation accuracy of the model is evaluated with a prototype.
3) A Bowden cable transmission system is developed for the LVSA to reduce the actuator's influence on the user's body mass distribution.
4) A torque-stiffness control method without force/torque sensor is proposed for the LVSA, and the performance of the controller is evaluated with a prototype.

The rest of this article is organized as follows: Section II introduces the mechanical design and working principles of LVSA. The modeling and analysis of LVSA are conducted in Section III. Section IV presents the performance test setup. The result of prototype test is reported and discussed in Sections V and VI, respectively. Finally, Section VII this article.

II. Design

The previous designs [13], [14] normally use one single elastic element as multiple elastic elements require more complicated mechanisms to ensure all the elastic elements can be adjusted by one motor. In the design with multiple elastic elements [26], [31], the stiffness adjuster generally employs multiple gears to control the elastic elements, which increases the complexity and weight of the actuator. This article proposed a novel mechanism, FS2C, to adjust the springs' preload, which reduces the weight and complexity of the stiffness regulation unit. The structure of the LVSA is shown in Fig. 1. There are two main units: 1) the unit A (compliant actuator unit) and 2) the unit B (stiffness regulation unit). The unit A has one FS2C consisting of four slider-crank mechanisms (SCMs) and four springs providing the actuator with inherent compliance. The rod A (shared crank of the FS2C A) is coupled with an input cable pulley of the unit A through the four springs. The unit B also has four SCMs connected with the distal ends of the four springs, respectively. All SCMs of the unit B are directly connected with one single shared crank (Rod B) so that the preload of all springs can be controlled together, which simplifies the mechanism of stiffness regulation. The slider of each SCM is guided by a caged ball linear guide to reduce friction. Two magnetic encoders are utilized to measure the deflection angle between the base plate and the rod A (output deflection angle, θ), and the base plate and rod B (unit B deflection angle, α). The range of stiffness of the LVSA is adjustable through the springs with various stiffnesses.

Connecting torsion springs in series with the input pulley can directly provide compliant actuation. However, this method requires complex mechanisms to achieve stiffness regulation. Previous studies use ball screws [20] and epicyclic gear [21] for stiffness regulation and result in bulky and heavy systems. In contrast, the FS2C of unit B enables simultaneously control of multiple springs, and the FS2C of unit A can convert linear motion of the springs to rotary motion of the output rod. Thus, the LVSA can achieve wider-range stiffness regulation with reduced weight.

A. Schematic of Variable Stiffness

Fig. 2 shows the schematic of the LVSA. There are four pairs of SCMs, and each pair has one SCM in the unit A and one SCM in unit B. The two SCMs are coupled through a spring which can generate torque against rod A when the output deflection angle $\theta \neq 0$. The value of this torque is determined by θ and the preload of the springs. Each slider of the SCM is physically restricted by two position limiters, ($|\overrightarrow{OQ}| < r_b + l_b$), thereby $\alpha \in (0, \alpha_{\max}]$. By adjusting α, the output torque can be changed without changing θ, which makes the stiffness of the LVSA adjustable.

To reduce the weight of the LVSA, a Bowden cable transmission system is designed to deliver the torque for both the unit A and the unit B. Two dc motors and gear boxes are used to drive the cable pulleys, separately. Each pair of dc motors and gearbox can provide 8 Nm continuously. All the segments are made by computer numerical control machines using Aluminum 7075.

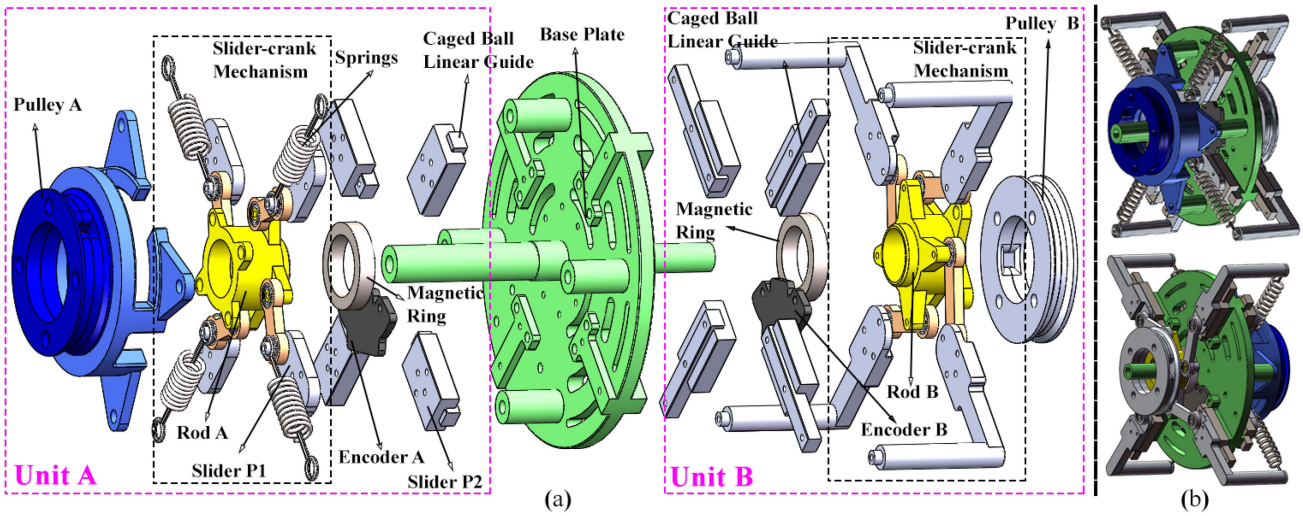

Fig. 1. (a) Explode view of the LVSA. The unit A is the main compliant actuator unit. The unit B is the stiffness regulation unit. Rod A is the output rod of the unit A. Rod B is the input rod of the unit B. Each slider is consist of one slider P1 and one slider P2. The P1 is attached to the P2 by screws, and they are considered as a rigid segment as a whole. (b) Assembly views of the LVSA.

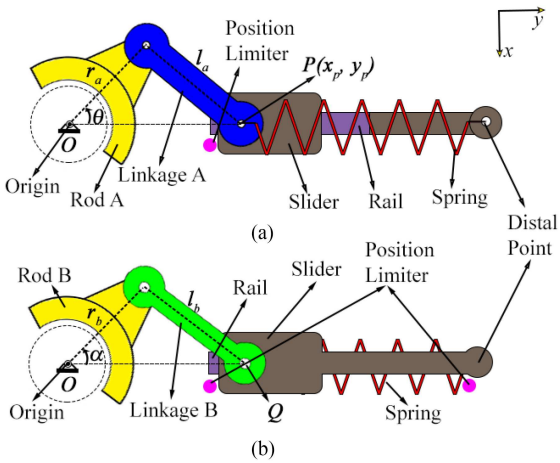

Fig. 2. Schematic of one branch of the LVSA. The rotation of the unit B input rod changes the position of the distal fix point, by which the preload of the springs can be regulated.

The weight of the LVSA prototype is reduced to 0.412 kg. The performance of the prototype will be evaluated in Sections V and VI.

III. Analysis of LVSA

A. Stiffness Modeling

To enhance the control of the LVSA, the torque-deflection and stiffness-deflection relations must be established. Thus, the following assumptions are made to facilitate the modeling.

Assumption 1: All segments in SCMs are considered as rigid.

Assumption 2: The stiffness of all springs are constant.

Assumption 3: The friction is negligible.

Let the length of Linkage A and B be l_a and l_b, respectively. The movement kinematics can be modeled as

$$r_a^2 \sin^2\theta + (y_p - r_a\cos\theta)^2 = l_a^2 \tag{1}$$

where $(0, y_p)$ is the position of P in frame O.

The output torque of the actuator can be formulated as

$$\tau = \sum_{i=1}^{N} (F_{s,i} r_{eq,i}) \tag{2}$$

where N is the number of springs; $F_{s,i}$ represents the force of the ith spring; $r_{eq,i}$ is the equivalent moment arm of $F_{s,i}$ against the output shaft, $r_{eq,1} = r_{eq,2} = r_{eq,3} = r_{eq,4} = r_{eq}(\theta)$ [which is defined in (6)]. $F_{s,i}$ can be obtained by

$$F_{s,i} = k_{s,i} l_{s,i} \tag{3}$$

where $k_{s,i}$ and $l_{s,i}$ is the stiffness and stretched length of the ith springs, respectively; $l_{s,1} = l_{s,2} = l_{s,3} = l_{s,4} = l_s(\theta, \alpha)$. According to (1), l_s can be calculated as

$$l_s(\theta, \alpha) = r_a + l_a - r_a\cos\theta - \sqrt{l_a^2 - r_a^2\sin^2\theta} + s(\alpha) \tag{4}$$

where s is the prestretched length of the springs which can be calculated as

$$s(\alpha) = r_b\cos\alpha + \sqrt{l_b^2 - (r_b\sin\alpha)^2} - r_b\cos\alpha_0 - \sqrt{l_b^2 - (r_b\sin\alpha_0)^2} \tag{5}$$

where α_0 is the initial deflection angle when the sliders of the unit B reach the proximal position limiters. Thus, the output torque τ changes with α. According to [42], the equivalent moment arm can be calculated as

$$r_{eq}(\theta) = \frac{r_a\left(r_a\sin\theta\cos\theta + \sin\theta\sqrt{l_a^2 - (r_a\sin\theta)^2}\right)}{\sqrt{l_a^2 - (r_a\sin\theta)^2}}. \tag{6}$$

The equivalent rotational stiffness of output shaft k_{eq} is defined by

$$\delta\tau = k_{eq}\delta\theta. \tag{7}$$

Let $F_s = \sum_{i=1}^{N} F_{s,i}$, it follows that

$$k_{eq}(\alpha,\theta) = \frac{\delta\tau}{\delta\theta} = r_{eq}\frac{\delta F_s}{\delta\theta} + F_s\frac{\delta r_{eq}}{\delta\theta} = \sum_{i=1}^{N} k_{s,i}\left(r_{eq}\frac{\delta l_s}{\delta\theta} + l_s\frac{\delta r_{eq}}{\delta\theta}\right). \tag{8}$$

Let $f_1 = r_{eq}\frac{\delta l_s}{\delta\theta}$, $f_2 = l_s\frac{\delta r_{eq}}{\delta\theta}$, then

$$\frac{\delta k_{eq}}{\delta\theta} = \sum_{i=1}^{N} k_{s,i}\left(\frac{\delta f_1}{\delta\theta} + \frac{\delta f_2}{\delta\theta}\right). \tag{9}$$

Thus, let $f_3 = \frac{\delta k_{eq}}{\delta\theta}$, the following relation can be found:

$$\begin{aligned} f_3 &> 0, \quad \text{for } \theta \in [0, \theta_{\max}] \\ f_3 &< 0, \quad \text{for } \theta \in [-\theta_{\max}, 0] \end{aligned} \tag{10}$$

where $\theta_{\max}$ is the maximal output deflection angle, and this means that the stiffness of the actuator increases with the rod A's absolute deflection angle. Similarly, it is easy to know that the stiffness of the actuator increases with the prestretched length $l_{s,i}$ and using (4) and (5)

$$\frac{\delta l_{s,i}}{\delta\alpha} < 0, \quad \text{for } \alpha \in [\alpha_{\min}, \alpha_0] \tag{11}$$

where $\alpha_{\min}$ is the rod B's deflection angle where the sliders of the unit B reach the distal position limiters, and $\alpha_{\min} > 0$.

B. Stiffness Range Reconfiguration

From Section III-A, the boundary of stiffness of the compliant actuator is determined by four linear factors $k_{s,i}$ and two nonlinear factors f_1, f_2. Reconfiguring springs (change the equivalent paralleled stiffness, $\sum_{i=1}^{N} k_{s,i}$) will change the lower and upper stiffness boundary of the actuator, which indicates that the LVSA can be adapted to different working environments simply by replacing springs. Thus, theoretically, the stiffness range is from 0 to ∞. However, due to the physical limitation of the material, the maximal output stiffness of the VSA is around 988 Nm/rad. In this study, the following two spring configurations will be tested: 1) $k_{s,1} = k_{s,2} = k_{s,3} = k_{s,4} = 3010$ N/m; 2) $k_{s,1} = k_{s,2} = k_{s,3} = k_{s,4} = 7000$ N/m.

C. Output Torque Estimation

Output torque estimation is important for torque control without force/torque sensor. Since the assembly error of the springs is inevitable, the model in Section III-A is modified for output torque estimation. The following assumption is adopted.

Assumption 4: The change of assembly errors of the springs are negligible.

Let the springs' assembly error be s_1, s_2, s_3, s_4. The average assembly error is defined as

$$s_e = \frac{\sum_{i=1}^{N} s_i}{N}. \tag{12}$$

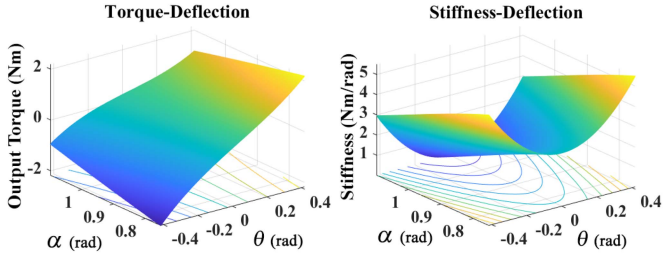

Fig. 3. Torque-deflection and stiffness-deflection relation from simulation when the springs' inherent stiffness $k_s = 3010$ N/m.

Thus, the compensated stretched length of springs can be obtained by

$$l_{\text{comp},i}(\theta,\alpha) = l_s(\alpha,\theta) + s_i \tag{13}$$

so that the output

$$\tau = \int k_{\text{eqc}}(\alpha,\theta)d\theta \tag{14}$$

where k_{eqc} is the compensated equivalent stiffness. Thus

$$k_{\text{eqc}} = \sum_{i=1}^{N} k_{s,i}\left(r_{eq}\frac{\delta l_{\text{comp},i}}{\delta\theta} + l_{\text{comp},i}\frac{\delta r_{eq}}{\delta\theta}\right). \tag{15}$$

Then, when the stiffness of the four springs are the same, the following equation can be found:

$$\begin{aligned} k_{\text{eqc}} &= \sum_{i=1}^{N} k_s\left(r_{eq}\frac{\delta l_{\text{comp},i}}{\delta\theta} + l_{\text{comp},i}\frac{\delta r_{eq}}{\delta\theta}\right) \\ &= \sum_{i=1}^{N} k_s\left(r_{eq}\frac{\delta l_s}{\delta\theta} + l_s\frac{\delta r_{eq}}{\delta\theta}\right) + k_s\frac{\delta r_{eq}}{\delta\theta}\sum_{i=1}^{N} s_i \\ &= k_{eq} + k_s\frac{\delta r_{eq}}{\delta\theta}Ns_e. \end{aligned} \tag{16}$$

Therefore, for the compensated model, only the average assembly error s_e needs to be determined when the stiffness of springs are the same.

D. Torque-Stiffness Control

Based on Section III-A the output torque τ and joint stiffness k_{eq} are determined by α and θ. Fig. 3 illustrates the simulated relationship between the output torque and the deflection angles.

Thus, the output torque and stiffness can be controlled by controlling the two deflection angles which can be determined by solving the following equations:

$$\begin{cases} k_{eq}(\alpha,\theta) = k_{eq,\,\text{des}} \\ \tau(\alpha,\theta) = \tau_{\text{des}}. \end{cases} \tag{17}$$

Fig. 4 depicts the paradigm of the torque-stiffness controller, where the PID controller A is used to control the rod B's deflection angle, and the PID controller B is used to manage the rod A's deflection angle. Both PID controllers are based on an inner closed-loop speed control of the motor, and the feedback only considers the real-time α, θ.

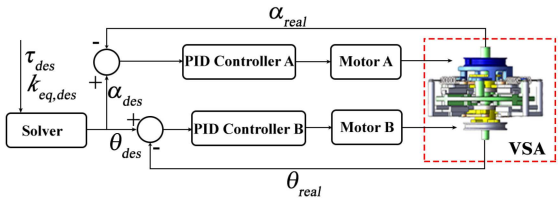

Fig. 4. Torque-stiffness controller paradigm of the LVSA. τ_{des} and $k_{eq,\text{des}}$ are the desired output torque and desired equivalent stiffness, respectively. α_{des} and θ_{des} are the desired deflection angles. α_{real} and θ_{real} are the measured deflection angles.

To reduce the computational cost of solving (17) and achieve a better real-time torque stiffness tracking, the following polynomials are used to approximate (17)

$$\begin{cases} k_{eq}(\alpha,\theta) & = p_0 + p_1\theta + p_2\alpha + p_3\alpha^2 + p_4\theta^2 \\ & \quad + p_5\theta\alpha + p_6\alpha^3 + p_7\theta^3 + p_8\alpha^2\theta + p_9\alpha\theta^2 \\ \tau(\alpha,\theta) & = q_0 + q_1\theta + q_2\alpha + q_3\alpha^2 + q_4\theta^2 \\ & \quad + q_5\theta\alpha + q_6\alpha^3 + q_7\theta^3 + q_8\alpha^2\theta + q_9\alpha\theta^2. \end{cases} \tag{18}$$

Based on the torque-deflection-angle and the stiffness-deflection data p_i, and q_i in (18) can be identified. Solving (18) can be converted to a nonlinear least-squares problem

$$\begin{aligned} &\arg\min_{\alpha,\theta} f(\alpha,\theta) = (k_{eq} - k_{eq,\text{des}})^2 + (\tau - \tau_{\text{des}})^2 \\ &\text{s.t.} \quad \alpha_{\min} < \alpha < \alpha_0 \\ &\qquad -\theta_{\max} < \theta < \theta_{\max}. \end{aligned} \tag{19}$$

Then, this optimization problem is solved using the Gauss–Newton method.

The open-loop dynamics of the VSA for torque control is simplified as a mass-damper-spring model. The transfer functions are identified using the Matlab System Identification Toolbox with a variance-accounted-for factor of 88.67%. The PID controllers are then designed based on the identified model.

IV. Prototype Experiments Setup

Fig. 5 left shows the prototype of the LVSA. The right side is the test setup for the performance evaluation, where the torque is transmitted through the Bowden cables to reduce the moment inertia of the actuation system. For both the unit A and B, there is one end fixer on the motor side and one on the LVSA side. The related modules are fixed on an aluminium framework, and all fixers are 3-D printed, including the motor base, Bowden cable fixed ends, and the VSA fixer. The rod A is coupled with a torque sensor which measures the real-time output torque at 500 Hz. In this study, three types of Bowden cable transmission systems are tested: 1) fishing wire and plastic Bowden tube; 2) steel wire and plastic Bowden tube; 3) steel wire and rubber Bowden tube with spiral sheaths. With type c Bowden cable, the motors achieved the control of the deflection angles with the shortest time and highest accuracy. Hence, the LVSA performance evaluation is based on type c Bowden cable transmission.

To evaluate the LVSA's performance, the PID controllers for the deflection angles control are assessed at first. Then,

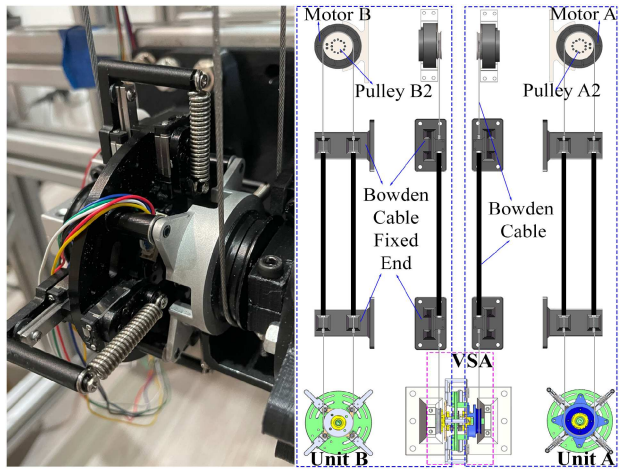

Fig. 5. Left: prototype of the VSA. Right: setup for performance test.

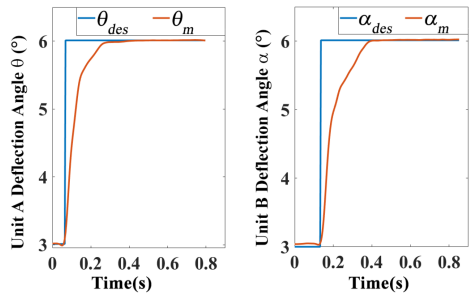

Fig. 6. Test result of the two PID controller in regulation the deflection angels.

there are five groups of test in the static evaluation to assess the torque-deflection angle θ relations for the rob B deflection angle α at 0°, 10°, and 20° for k_s = 300 N/m, and at 0°, 3°, and 6° for k_s = 7000 N/m, respectively. Each group contains four repetitive tests, and for each tests, the output torque and deflection angles are recorded. Finally, the dynamic test is taken to evaluate the dynamic torque estimation and torque-stiffness tracking accuracy, the controller is required to track a sinusoidal desired torque with a constant desired stiffness.

V. Results

A. Deflection Angle Control

The deflection angles are controlled by two PID controllers separately, which is the basis of the performance evaluation. Thus, the PID controllers are first tested in regulating the deflection angles. The result is shown in Fig. 6, where the rise time of both PID controllers is around 200 ms.

B. Compensation Evaluation

As mentioned in Section IV, the static evaluation contains five groups of test, which aim to identify the torque/deflection angle relation and compare it with the estimated result. For each group of the test, one test data will be used to approximate compensation parameters in Section III-C. Thus, the model

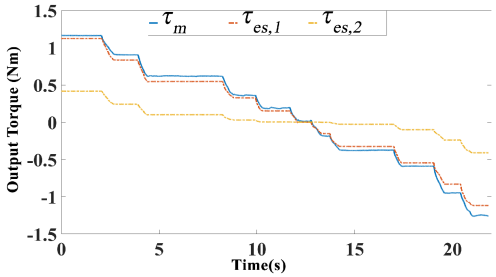

Fig. 7. Comparison of the output torque estimation between the compensated and noncompensated model. τ_m is the measured torque, $\tau_{es,1}$ and $\tau_{es,2}$ are the torque estimated by the compensated model, and the torque estimated by the noncompensated model, respectively.

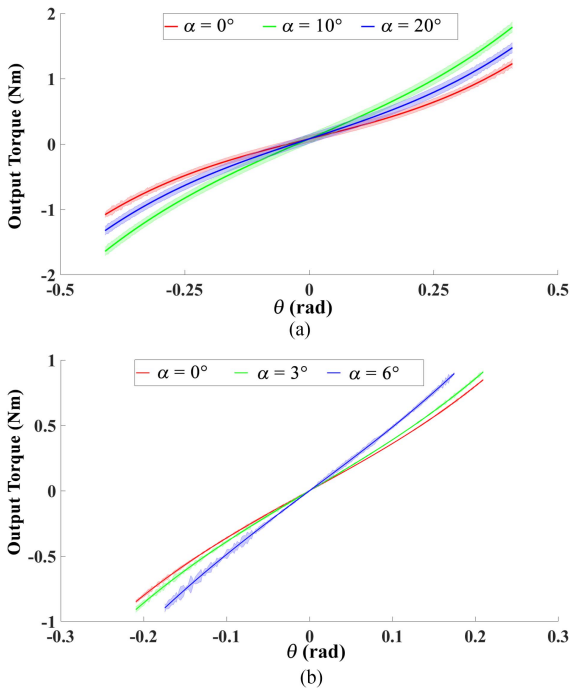

Fig. 8. Output torque estimation of the LVSA, solid lines represent the model's estimation and the shaded area is the range of the measured torque. $k_s = 3010$ N/m in (a), and $k_s = 7000$ N/m in (b).

presented in (14) and (16) can be identified. Fig. 7 shows the comparison between the ideal model and the compensated model in output torque estimation.

C. Static Evaluation

The data of the rest three tests of each group is utilized to estimate the output torque with the compensated model [(14) and (16)]. To evaluate the model's estimation accuracy, the estimation results are compared with the measured output torque. Fig. 8 shows the comparison between the model estimation and the measured output torque for two different configurations of springs. The torque estimation accuracy is quantified by the root-mean-squared error (RMSE) which is defined as

$$\text{RMSE} = \sqrt{\frac{1}{N}\sum_{i=1}^{N}(a_i - \widehat{a}_i)^2} \tag{20}$$

TABLE I
MEAN RMSE VALUES BETWEEN THE MEASURED TORQUE AND ESTIMATED TORQUE

k_s (N/m)	RMSE_1	RMSE_2	RMSE_3	Average
3010	0.0564	0.1143	0.1176	0.0961
7000	0.0353	0.0450	0.0447	0.0417

All values are in Nm
RMSE_1: $\alpha = 0°$ for both $k_s = 3010$ N/m and $k_s = 7000$ N/m
RMSE_2: $\alpha = 10°$ for $k_s = 3010$ N/m, $\alpha = 3°$ for $k_s = 7000$ N/m
RMSE_3: $\alpha = 20°$ for $k_s = 3010$ N/m, $\alpha = 6°$ for $k_s = 7000$ N/m

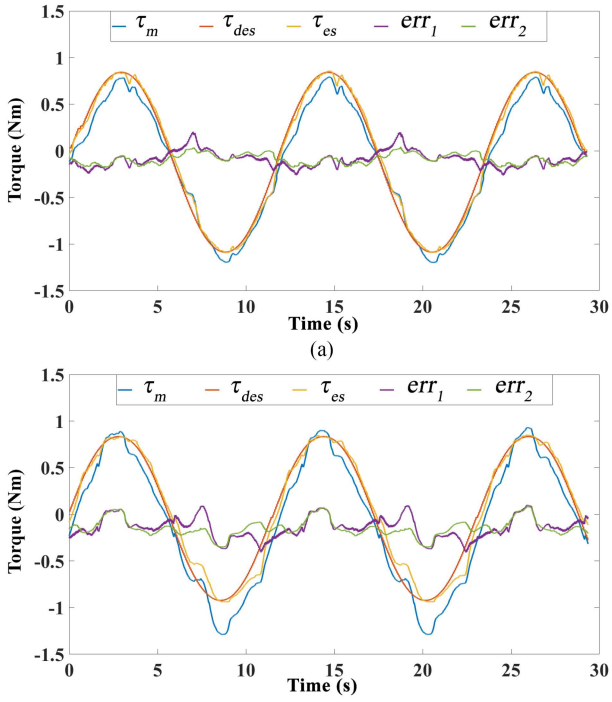

Fig. 9. Torque tracking test. τ_m: measured torque, τ_{des}: desired torque, τ_{es}: estimated torque, err_1: error between the measured and desired torque, err_2: error between the measured and estimated torque. $k_s = 3010$ N/m in (a), and $k_s = 7000$ N/m in (b).

where a_i is the measured torque, and $\widehat{a}_i$ is the torque estimated by the model. Table I summarizes the estimation accuracy for different tests.

D. Torque Tracking Test

In the torque tracking test, the LVSA is set to track a sinusoidal desired output torque with constant stiffness. As mentioned in Section III-D, the solver will calculate the desired deflection angles with the desired torque and stiffness. Then, the inner loop PID controllers control the motors to achieve the desired deflection angles, and the torque sensor measures the real-time output torque. The comparison results between the real-time torque and desired torque for both sets of springs are illustrated in Fig. 9.

It is difficult to measure the real-time output stiffness of the actuator, and thereby the output stiffness is calculated using (16) based on the measured deflection angles. Fig. 10 illustrates the comparison between the estimated stiffness and desired stiffness.

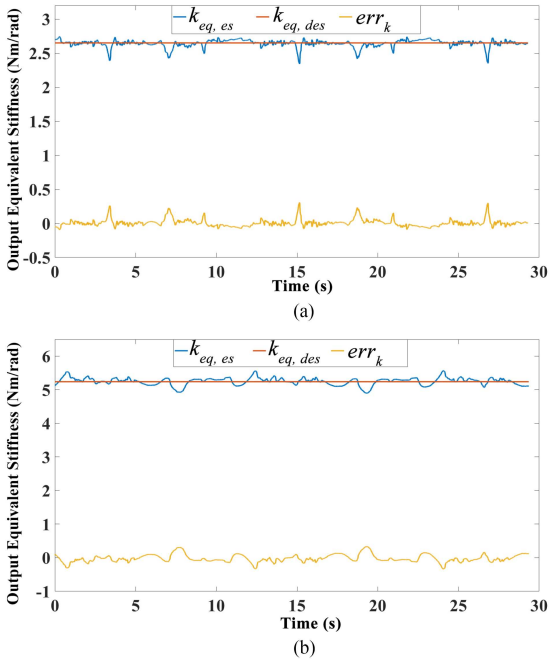

Fig. 10. Stiffness tracking test. $k_{eq,es}$ and $k_{eq,des}$ are the estimated and desired equivalent stiffness, respectively. err_k is the error between the desired and estimated equivalent stiffness. $k_s = 3010$ N/m in (a), and $k_s = 7000$ N/m in (b).

TABLE II
RMSE VALUES FOR QUANTIFY THE TORQUE TRACKING ACCURACY, DYNAMIC TORQUE ESTIMATION ACCURACY AND THE STIFFNESS TRACKING ACCURACY

k_s (N/m)	$\text{RMSE}_{\tau,1}$(Nm)	$\text{RMSE}_{\tau,2}$(Nm)	RMSE_k(Nm/rad)
3010	0.1222	0.1046	0.0561
7000	0.1829	0.1723	0.1128

The RMSE between the measured and desired output torque is identified as $\text{RMSE}_{\tau,1}$. Then, the RMSE between the estimated and measured torque is calculated to quantify the dynamic torque estimation accuracy $\text{RMSE}_{\tau,2}$, and the RMSE between the estimated and desired stiffness is computed to quantify the stiffness tracking performance RMSE_k. Table II summarizes the RMSE values for the two sets of springs.

E. Stiffness Regulation Evaluation

In pHRI, the environmental changes require the change of stiffness to ensure the safety and robustness, and the stiffness regulation speed is the crucial feature reflecting how fast the actuator can respond the environmental changes. Thus, the stiffness regulation test is taken to evaluate the respond speed of the proposed LVSA. In this test, the desired stiffness is rapidly changed, and the controller is required to respond immediately to reach desired stiffness. The result is shown in Fig. 11 where the regulation time of the stiffness is around 220 ms for (a) $k_s = 3010$ N/m, and is around 420 ms for (b) $k_s = 7000$ N/m.

VI. DISCUSSION

According to Fig. 6, the PID controller for both the unit A and B can control the machine to the desired deflection angles in a promising time period within a reasonable range. It indicates that the controller is adequate for the performance evaluation test. Section V-B assesses the compensated model's performance in output torque estimation. The result reveals that the compensated model improves the estimation accuracy significantly, which means that the compensated model can effectively reduce the impact of the assembling error.

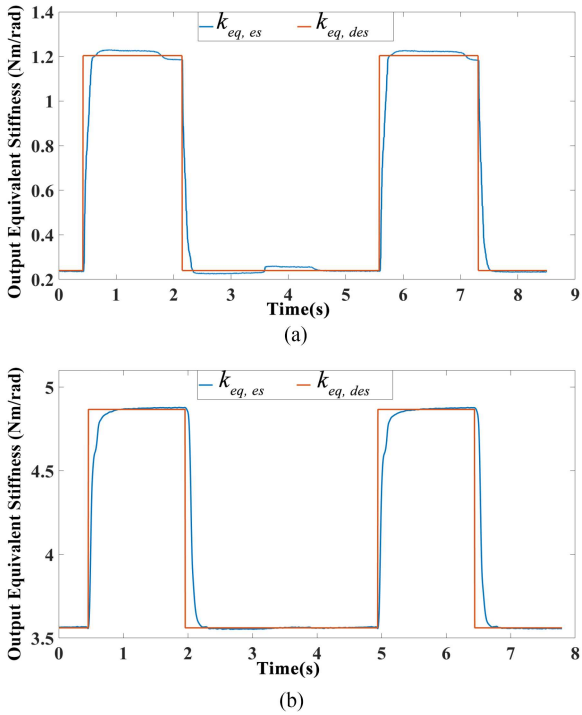

Fig. 11. Stiffness regulation test: the actuator is required the change between two different equivalent output stiffness. $k_s = 3010$ N/m in (a), and $k_s = 7000$ N/m in (b).

The result of the static evaluation demonstrates that the output torque for the same deflection angle can be adjusted, which means that the stiffness adjustment can be achieved by the proposed design. The shaded error range indicates that our model can accurately estimate the output torque based on the deflection angles for different spring configurations. However, from Fig. 8(a), the output torque is only tested from -2 to 2 Nm; the reason is that the components holding the two ends of the springs are made of Aluminium 7075 whose yield strength is small so that it cannot carry too much load. Similarly, for $k_s = 7000$ N/m, the output torque is tested from -1 to 1 Nm, which is smaller than that for $k_s = 3010$ N/m. This is because the stiffer springs can produce the same stretch force with a smaller stretch length so that the stiffer spring can reach maximal secure force at a smaller deflection angle.

The inherent torque-stiffness-deflection relations of the LVSA and the encoders allow the controller to estimate its output torque and stiffness, which makes the torque-stiffness control without force/torque sensor possible. The caged ball linear guide mechanisms are employed to work with the SCMs to reduce the friction's impact on the output torque and stiffness. Fig. 9 illustrates the LVSA torque tracking for two different sets of springs. For $k_s = 3010$ N/m, the RMSE of torque tracking is about 0.1222 Nm; and for $k_s = 7000$ N/m the torque tracking

TABLE III
COMPARISON OF THE OPERATING SPECIFICATIONS OF SERIAL VSAS

Name	Mass (kg)	Range of Stiffness (Nm/rad)	Stiffness Regulation Time (s)	Range of Motion (∘)	Range of Deflection(∘)	Nominal Torque(Nm)	Peak Torque(Nm)
MACCEPA 2.0 [18]	2.4	5∼110	2.6	±150	0∼60	50	70
AwAS-II [20]	1.1	0∼∞	0.8	±150	±17	10.75	80
vsaUT-II [44]	2.5	0.7∼948	-	±28.6	±40.1	21.8	60
SVSA [24]	1.57	1.7∼150	0.4	±180	±45	9.46	22.1
RVSA [19]	2.0	3.5∼426	0.38	0∼135	±20	19	66.6
LVSA	**0.41**	**0∼988**	**0.22**	**±180**	**±25**	**2.5**	**3.8**

RMSE is about 0.1829 Nm. The RMSE values for both sets of springs are relatively low, which indicates the LVSA can track the desired output torque and stiffness accurately with two encoders. However, the err_2 lines in Fig. 9 indicate that the error is position-related, and the error is significantly higher than the error presented in the static evaluation. This may be caused by the deformation of the 3-D-printed fixed end of the Bowden cable and the LVSA housing segment. From the performance test setup, it is easy to know that the force on the Bowden cable is applied to the LVSA housing, which may cause noticeable deformation. This deformation should be related to the value of the force applied by the Bowden cable. In the static evaluation, the torque and deflection angle are measured in the static positions, while in the torque tracking test, the two input shafts are running at a relatively high acceleration, which means that the force on the Bowden cable is higher than the static evaluation. Therefore, the deformation in the torque tracking test is higher, which causes a larger decentration for the LVSA performance evaluation setup. Combining err_1 and err_2, the torque tracking error is larger than the dynamic estimation, which is reasonable as the dynamic estimation is the basis of torque tracking. However, this also indicates that the controller needs to be improved to respond quickly. It is difficult to measure the online stiffness of the LVSA, thus the estimated stiffness is only compared with the desired stiffness, the result is obtained in Fig. 10 and Table II, the RMSE value for stiffness tracking is 0.0561 and 0.1128 Nm/rad for $k_s = 3010$ N/m and $k_s = 7000$ N/m, respectively. Even the result demonstrates that the proposed controller can achieve stiffness tracking with promising accuracy. However, the torque tracking error for stiffer springs is higher than for softer springs. The reason is that the maximal deflection angles decrease with the raise of spring stiffness; thus, the error rate of deflection angle measurement is increased with stiffer springs, which decreases the estimation accuracy. Hence, it is important to improve the accuracy of deflection angle measurement, such as using high-resolution encoders and strain gauges.

The stiffness regulation test aims to evaluate the response speed of the actuator and controller to environment changes. The results show that the output stiffness is quickly regulated for both $k_s = 3010$ N/m and $k_s = 7000$ N/m. However, for the stiffer springs, the regulation time is longer. The reason is that the output torque of the motor is very close to its allowed maximal value, and the motor cannot run at the speed set by the PID controller. Consequently, the rise time of the stiffness regulation for stiffer springs is significantly longer. Beside, the Bowden cable transmission system of unit B produces a resistance torque against the shaft on the base plate, which limits the stiffness adjustment range and output torque of the LVSA. Therefore, to improve the performance of the LVSA, the power transmitted from motor B to the adjuster should be increased, and the power producing the resistance torque should be minimized. A potential solution is designing a decoupling mechanism for unit B, by which the the Bowden cable always points toward the center of base plate shaft resulting zero resistance torque.

In addition, if the external torque exceeds the holding torque of motor B, unit B will be moved passively. In this study, we employed a dc motor with a high holding torque for unit B and the output of motor A is limited in software to ensure the external torque will not exceed the holding torque of motor B. A self-locking mechanism can be further added to remove the requirement on the holding torque.

With a weight of 0.412 kg, the LVSA can be potentially used in the actuation of rehabilitation exoskeletons. The lightweight of the LVSA has small influences on the body mass distribution, which reduces the risk of developing abnormal motor patterns [16]. A wider-range stiffness adaption and torque control can contribute to safe human–robot interaction and flexible training strategies.

VII. CONCLUSION

In this article, a lightweight VSA was proposed on the basis of a novel mechanism named FS2C. The FS2C consists of four sliders on a shared crank, which allows the LVSA to simultaneously adjust the preload of the springs using one single motor. Hence, the LVSA achieved a wider-range stiffness adaption with a light weight, 0.412 kg, which is extremely low compared with the recently proposed VSAs, see Table III. The dynamics of the LVSA were modeled to study the torque-deflection and stiffness-deflection relations. The accuracy of the torque estimation of the dynamics model was evaluated, and the results showed the average accuracy (identified by the RMSE) for $k_s = 3010$ N/m is about 0.0961 Nm and for $k_s = 7000$ N/m is about 0.0417 Nm, see Table I. A torque-stiffness control method without force/torque sensor was proposed on the basis of the dynamics model, and its performance was evaluated with the prototype. The results demonstrated that the proposed LVSA achieved high-speed stiffness regulation (0.22 s for $k_s = 3010$ N/m, and 0.45 s for $k_s = 7000$ N/m), and the torque-stiffness tracking tests showed an encouraging accuracy, see Table II. Our study showed that the LVSA has several limitations: 1) the nominal output torque is relatively limited; 2) unit B might be moved passively if the external torque exceeds the holding

torque of motor B; 3) the tendon force of the Bowden cable of unit B not only produces a driving torque for the stiffness adjuster but also generates a resistance torque against the base plate shaft, which reduces the energy efficiency of motor B and limited the stiffness adjustment range. Future work will be adding velocity feedback for antidisturbance and advanced control and optimizing the mechanical structure of the LVSA to improve the performance of the actuator, such as developing a self-locking mechanism for motor B, designing a decoupling mechanism, by which the tendon force of Bowden cable of unit B always points to the rotary center of the base plate shaft resulting in zero resistance force and higher energy efficiency of motor B.

REFERENCES

[1] X. Cui, W. Chen, X. Jin, and S. Agrawal, "Design of a 7-DOF cable-driven arm exoskeleton (CAREX-7) and a controller for dexterous motion training or assistance," *IEEE/ASME Trans. Mechatron.*, vol. 22, no. 1, pp. 161–172, Feb. 2017.

[2] L. Bergmann et al., "Lower limb exoskeleton with compliant actuators: Design, modeling, and human torque estimation," *IEEE/ASME Trans. Mechatron.*, pp. 1–12, 2022.

[3] J. Pan et al., "NESM-γ: An upper-limb exoskeleton with compliant actuators for clinical deployment," *IEEE Robot. Autom. Lett.*, vol. 7, no. 3, pp. 7708–7715, Jul. 2022.

[4] J. Song, A. Zhu, Y. Tu, X. Zhang, and G. Cao, "Novel design and control of a crank-slider series elastic actuated knee exoskeleton for compliant human–robot interaction," *IEEE/ASME Trans. Mechatron.*, vol. 28, no. 1, pp. 531–542, Feb. 2023.

[5] A. Calanca and P. Fiorini, "On the role of compliance in force control," in *Proc. Intell. Auton. Syst.*, 2015, pp. 1243–1255.

[6] N. Hogan, "Contact and physical interaction," *Annu. Rev. Control Robot. Auton. Syst.*, vol. 5, no. 1, pp. 179–203, 2022.

[7] Y. Ayoubi, M. A. Laribi, M. Arsicault, and S. Zeghloul, "Safe pHRI via the variable stiffness safety-oriented mechanism (V2SOM): Simulation and experimental validations," *Appl. Sci.*, vol. 10, no. 11, 2020, Art. no. 3810.

[8] R. Bischoff et al., "The KUKA-DLR lightweight robot arm: A new reference platform for robotics research and manufacturing," in *Proc. 41st Int. Symp. Robot. 6th German Conf. Robot.*, 2010, pp. 1–8.

[9] G. Raiola, C. Cardenas, T. Tadele, T. de Vries, and S. Stramigioli, "Development of a safety- and energy-aware impedance controller for collaborative robots," *IEEE Robot. Autom. Lett.*, vol. 3, no. 2, pp. 1237–1244, Apr. 2018.

[10] K. Lee, S. Baek, H. Lee, H. Choi, H. Moon, and J. Koo, "Enhanced transparency for physical human-robot interaction using human hand impedance compensation," *IEEE/ASME Trans. Mechatron.*, vol. 23, no. 6, pp. 2662–2670, Dec. 2018.

[11] M. Cestari, D. Sanz-Merodio, J. Arevalo, and E. Garcia, "An adjustable compliant joint for lower-limb exoskeletons," *IEEE/ASME Trans. Mechatron.*, vol. 20, no. 2, pp. 889–898, Apr. 2015.

[12] A. Jafari, N. Tsagarakis, and D. Caldwell, "AwAS-II: A new actuator with adjustable stiffness based on the novel principle of adaptable pivot point and variable lever ratio," in *Proc. IEEE Int. Conf. Robot. Automat.*, 2011, pp. 4638–4643.

[13] B. Vanderborght, N. G. Tsagarakis, C. Semini, R. Van Ham, and D. G. Caldwell, "MACCEPA 2.0: Adjustable compliant actuator with stiffening characteristic for energy efficient hopping," in *Proc. IEEE Int. Conf. Robot. Automat.*, 2009, pp. 544–549.

[14] Z. Li, W. Chen, and S. Bai, "A novel reconfigurable revolute joint with adjustable stiffness," in *Proc. Int. Conf. Robot. Automat.*, 2019, pp. 8388–8393.

[15] L. Tiseni, G. Rinaldi, D. Chiaradia, and A. Frisoli, "Design and control of a linear springs-based rotary series elastic actuator for portable assistive exoskeletons," in *Proc. IEEE 30th Int. Conf. Robot Hum. Interactive Commun.*, 2021, pp. 434–439.

[16] T. Chen, R. Casas, and P. Lum, "An elbow exoskeleton for upper limb rehabilitation with series elastic actuator and cable-driven differential," *IEEE Trans. Robot.*, vol. 35, no. 6, pp. 1464–1474, Dec. 2019.

[17] G. A. Pratt and M. M. Williamson, "Series elastic actuators," in *Proc. IEEE/RSJ Int. Conf. Intell. Robots Syst. Hum. Robot. Interact. Cooperative Robots*, 1995, pp. 399–406.

[18] V. Grosu, C. Rodriguez-Guerrero, S. Grosu, B. Vanderborght, and D. Lefeber, "Design of smart modular variable stiffness actuators for robotic-assistive devices," *IEEE/ASME Trans. Mechatron.*, vol. 22, no. 4, pp. 1777–1785, Aug. 2017.

[19] Y. Zhu, Q. Wu, B. Chen, D. Xu, and Z. Shao, "Design and evaluation of a novel torque-controllable variable stiffness actuator with reconfigurability," *IEEE/ASME Trans. Mechatron.*, vol. 27, no. 1, pp. 292–303, Feb. 2022.

[20] A. Jafari, N. Tsagarakis, I. Sardellitti, and D. Caldwell, "A new actuator with adjustable stiffness based on a variable ratio lever mechanism," *IEEE/ASME Trans. Mechatron.*, vol. 19, no. 1, pp. 55–63, Feb. 2014.

[21] Z. Li, P. Xu, H. Huang, Y. Ning, and B. Li, "A novel variable stiffness actuator based on a rocker-linked epicyclic gear train," *Mechanism Mach. Theory*, vol. 177, 2022, Art. no. 105035.

[22] L. Visser, R. Carloni, F. Klijnstra, and S. Stramigioli, "A prototype of a novel energy efficient variable stiffness actuator," in *Proc. IEEE Annu. Int. Conf. Eng. Med. Biol.*, 2010, pp. 3703–3706.

[23] L. Visser, R. Carloni, and S. Stramigioli, "Energy-efficient variable stiffness actuators," *IEEE Trans. Robot.*, vol. 27, no. 5, pp. 865–875, Oct. 2011.

[24] J. Sun, Z. Guo, Y. Zhang, X. Xiao, and J. Tan, "A novel design of serial variable stiffness actuator based on an archimedean spiral relocation mechanism," *IEEE/ASME Trans. Mechatron.*, vol. 23, no. 5, pp. 2121–2131, Oct. 2018.

[25] K. W. Hollander, T. G. Sugar, and D. E. Herring, "Adjustable robotic tendon using a 'Jack Spring'," in *Proc. 9th Int. Conf. Rehabil. Robot.*, 2005, pp. 113–118.

[26] Y. Xu, K. Guo, J. Li, and Y. Li, "A novel rotational actuator with variable stiffness using S-shaped springs," *IEEE/ASME Trans. Mechatron.*, vol. 26, no. 4, pp. 2249–2260, Aug. 2021.

[27] E. Barrett, J. Malzahn, and N. Tsagarakis, "A compliant mechanism with progressive stiffness for robotic actuation," in *Proc. IEEE/ASME Int. Conf. Adv. Intell. Mech.*, 2021, pp. 774–780.

[28] Y. Sun, P. Tang, D. Dong, J. Zheng, X. Chen, and L. Bai, "Modeling and experimental evaluation of a pneumatic variable stiffness actuator," *IEEE/ASME Trans. Mechatron.*, vol. 27, no. 5, pp. 2462–2473, Oct. 2022.

[29] L. Miskovic, M. Dezman, and T. Petric, "Pneumatic quasi-passive variable stiffness mechanism for energy storage applications," *IEEE Robot. Autom. Lett.*, vol. 7, no. 2, pp. 1705–1712, Apr. 2022.

[30] S. Wolf et al., "Variable stiffness actuators: Review on design and components," *IEEE/ASME Trans. Mechatron.*, vol. 21, no. 5, pp. 2418–2430, Oct. 2016.

[31] X. Li, H. Zhu, W. Lin, W. Chen, and K. Low, "Structure-controlled variable stiffness robotic joint based on multiple rotary flexure hinges," *IEEE Trans. Ind. Electron.*, vol. 68, no. 12, pp. 12452–12461, Dec. 2021.

[32] M. Rahman, M. Rahman, O. Cristobal, M. Saad, J. Kenné, and P. Archambault, "Development of a whole arm wearable robotic exoskeleton for rehabilitation and to assist upper limb movements," *Robotica*, vol. 33, no. 1, pp. 19–39, 2014.

[33] E. Trigili et al., "Design and experimental characterization of a shoulder-elbow exoskeleton with compliant joints for post-stroke rehabilitation," *IEEE/ASME Trans. Mechatron.*, vol. 24, no. 4, pp. 1485–1496, Aug. 2019.

[34] A. Otten, C. Voort, A. Stienen, R. Aarts, E. van Asseldonk, and H. van der Kooij, "LIMPACT: A hydraulically powered self-aligning upper limb exoskeleton," *IEEE/ASME Trans. Mechatron.*, vol. 20, no. 5, pp. 2285–2298, Oct. 2015.

[35] K. Staman, A. Veale, and H. van der Kooij, "Design, control and evaluation of the electro-hydrostatic actuator, PREHydrA, for gait restoration exoskeleton technology," *IEEE Trans. Med. Robot. Bionics*, vol. 3, no. 1, pp. 156–165, Feb. 2021.

[36] C. Nycz, T. Butzer, O. Lambercy, J. Arata, G. Fischer, and R. Gassert, "Design and characterization of a lightweight and fully portable remote actuation system for use with a hand exoskeleton," *IEEE Robot. Autom. Lett.*, vol. 1, no. 2, pp. 976–983, Jul. 2016.

[37] J. Kuan, K. Pasch, and H. Herr, "A high-performance cable-drive module for the development of wearable devices," *IEEE/ASME Trans. Mechatron.*, vol. 23, no. 3, pp. 1238–1248, Jun. 2018.

[38] R. Hidayah, L. Bishop, X. Jin, S. Chamarthy, J. Stein, and S. K. Agrawal, "Gait adaptation using a cable-driven active leg exoskeleton (C-ALEX) with post-stroke participants," *IEEE Trans. Neural Syst. Rehabil. Eng.*, vol. 28, no. 9, pp. 1984–1993, Sep. 2020.

[39] B. Zhong, K. Guo, H. Yu, and M. Zhang, "Toward gait symmetry enhancement via a cable-driven exoskeleton powered by series elastic actuators," *IEEE Robot. Autom. Lett.*, vol. 7, no. 2, pp. 786–793, Apr. 2022.

[40] Y. Huang, Y. Chen, X. Zhang, H. Zhang, C. Song, and J. Ota, "A novel cable-driven 7-DOF anthropomorphic manipulator," *IEEE/ASME Trans. Mechatron.*, vol. 26, no. 4, pp. 2174–2185, Aug. 2021.
[41] Z. Li et al., "A novel cable-driven antagonistic joint designed with variable stiffness mechanisms," *Mechanism Mach. Theory*, vol. 171, 2022, Art. no. 104716.
[42] Y. H. Zweiri, J. F. Whidborne, and L. D. Seneviratne, "Instantaneous friction components model for transient engine operation," *Proc. Inst. Mech. Eng., Part D: J. Automobile Eng.*, vol. 214, no. 7, pp. 809–824, Jul. 2000.
[43] C. W. Mathews and D. J. Braun, "Design of parallel variable stiffness actuators," *IEEE Trans. Robot.*, vol. 39, no. 1, pp. 768–782, Feb. 2023.
[44] S. Groothuis, G. Rusticelli, A. Zucchelli, S. Stramigioli, and R. Carloni, "The variable stiffness actuator vsaUT-II: Mechanical design, modeling, and identification," *IEEE/ASME Trans. Mechatron.*, vol. 19, no. 2, pp. 589–597, Apr. 2014.

Chao Wang received the B.Eng. degree in electrical engineering from the Zhengzhou University, Henan, China, in 2017. He is currently working toward the Ph.D. degree in the mechatronics with the School of Electronic and Electrical Engineering, University of Leeds, Leeds, U.K.

His research interests include human–robot interaction, compliant actuation systems, and rehabilitation robotics.

Bo Sheng received the M.Eng. degree in mechatronics from the Huazhong University of Science and Technology, Wuhan, China, in 2014, and the Ph.D. degree in mechanical engineering from the University of Auckland, Auckland, New Zealand, in 2019.

From 2019 to 2021, he was a Research Associate with the Department of Exercise Sciences, University of Auckland. He is currently a Lecturer with the School of Mechatronic Engineering and Automation, Shanghai University, Shanghai, China. He has participated in more than ten research projects in areas of rehabilitation robots, interaction control, and medical informatics. He has authored more than 26 academic journal and conference papers. His research interests include robot-assisted rehabilitation, human–robot interaction, and medical informatics

Zhenhong Li (Member, IEEE) received the B.Eng. degree in electrical engineering from the Huazhong University of Science and Technology, Wuhan, China, and the M.S. and Ph.D. degrees in control engineering from the University of Manchester, Manchester, U.K., in 2014 and 2019, respectively.

From 2018 to 2019, he was a Research Associate with the University of Manchester. He is currently a Research Fellow with the School of Electronic and Electrical Engineering, University of Leeds, Leeds, U.K. His research interests include distributed optimization, and cooperative control of multiagent systems.

Manoj Sivan received the M.D. degree from University of Leeds, Leeds, U.K., in 2014. He is an Associate Clinical Professor and Honorary Consultant in Rehabilitation Medicine (RM) with University of Leeds, Leeds, U.K., and Leeds NHS Trusts. He is an advisor for the World Health Organisation (WHO) for its Covid rehabilitation policy in Europe. His work is supported by research grants from NIHR, MRC, EPSRC, ISRT, Research England and RCP. His research interests are rehabilitation technology, health services, upper limb rehabilitation, chronic pain, and outcome measurement .

Dr. Sivan was the recipient of the prestigious European Academy and Philip Nichols awards in 2014 for his research in upper limb rehabilitation robotics. His Covid rehabilitation work won his team the 2021 BMJ Clinical Leadership Team award and the digital application C19-YRS system he helped develop won the 2021 Medipex NHS Innovation award. He is the Editor-in-Chief (EIC) for the journal *Rehabilitation Process and Outcome* and the EIC for the *Oxford Handbook of Rehabilitation Medicine*.

Zhi-Qiang Zhang (Member, IEEE) received the Ph.D. degree in electrical engineering from the University of Chinese Academy of Sciences, Beijing, China, in 2010.

He was a Research Associate with Imperial College London, London, U.K., for five and half years. He is an Associate Professor of Body Sensor Networks for healthcare and robotic control with the University of Leeds, Leeds, U.K. He has authored or coauthored more than 50 papers in peer-reviewed publications. His research interests are human kinematics, musculoskeletal modeling, and machine learning.

Gu-Qiang Li received the M.Sc. degree in sport body science from the Jiangsu Normal University, Xuzhou, China, in 2008.

He is currently an Associate Professor with the School of Rehabilitation Medicine, Binzhou Medical University, Yantai, China. His research interests include rehabilitation robotics, intelligent rehabilitation assistive devices, and 3-D-printed orthosis in the clinic.

Sheng Quan Xie (Senior Member, IEEE) received the Ph.D. degree in mechanical engineering from the University of Canterbury, Christchurch, New Zealand, in 2002.

In 2003, he joined the University of Auckland, Auckland, New Zealand, and became a Chair Professor in (Bio) mechatronics in 2011. Since 2017, he has been the Chair of Robotics and Autonomous Systems with the University of Leeds, Leeds, U.K. He has authored or coauthored eight books, 15 book chapters, and more than 400 international journal and conference papers. His research interests include medical and rehabilitation robots and advanced robot control.

Dr. Xie is an Elected Fellow of The Institution of Professional Engineers New Zealand.